Available online at www.sciencedirect.com
ScienceDirect
Magnetic Resonance Imaging 27 (2009) 480–488
MAGNETIC RESONANCE IMAGING

GRAPPA-based susceptibility-weighted imaging of normal volunteers and patients with brain tumor at 7 T☆

Janine M. Lupo[a,*], Suchandrima Banerjee[a,b,1], Kathryn E. Hammond[a,b], Douglas A.C. Kelley[c], Duan Xu[a], Susan M. Chang[d], Daniel B. Vigneron[a,e], Sharmila Majumdar[a,e], Sarah J. Nelson[a,e]

[a]Department of Radiology, Surbeck Laboratory of Advanced Imaging, University of California, San Francisco, CA 94158-2532, USA
[b]UCSF/UCB Joint Graduate Group in Bioengineering, University of California, San Francisco, CA 94158-2532, USA
[c]GE Healthcare Technologies, Global Applied Science Laboratory, San Francisco, CA 94158-2532, USA
[d]Department of Neurosurgery, University of California, San Francisco, CA 94158-2532, USA
[e]Program in Bioengineering, University of California, San Francisco, CA 94158-2532, USA

Received 19 December 2007; revised 14 August 2008; accepted 14 August 2008

Abstract

Susceptibility-weighted imaging (SWI) is a valuable technique for high-resolution imaging of brain vasculature that greatly benefits from the emergence of higher field strength MR scanners. Autocalibrating partially parallel imaging techniques can be employed to reduce lengthy acquisition times as long as the decrease in signal-to-noise ratio does not significantly affect the contrast between vessels and brain parenchyma. This study assessed the feasibility of a Generalized Autocalibrating Partially Parallel Acquisition (GRAPPA)-based SWI technique at 7 T in both healthy volunteers and brain tumor patients. GRAPPA-based SWI allowed a twofold or more reduction in scan time without compromising vessel contrast and small vessel detection. Postprocessing parameters for the SWI needed to be modified for patients where the tumor causes high-frequency phase wrap artifacts but did not adversely affect vessel contrast. GRAPPA-based SWI at 7 T revealed regions of microvascularity, hemorrhage and calcification within heterogeneous brain tumors that may aid in characterizing active or necrotic tumor and monitoring treatment effects.
Published by Elsevier Inc.

Keywords: SWI; 7 T; Parallel imaging; Brain tumor

1. Introduction

Susceptibility-weighted imaging (SWI) is a powerful tool for high-resolution imaging of the vasculature [1] that has been shown to improve the diagnosis of many pathologic conditions at low field strengths, including brain neoplasms, neurological trauma, vascular malformations and a variety of cerebrovascular and neurodegenerative diseases [2,3]. The signal loss that creates contrast in the magnitude image arises due to intravoxel dephasing and partial volume effects near venous vessels, typically requiring long echo times (TEs). The additional weighting relies on changes in phase that result from susceptibility effects of deoxygenated blood in venous vessels. With this technique, postprocessing of the phase information is used to amplify magnitude image contrast between tissues that have different susceptibilities.

SWI is expected to be important for measuring blood volume at higher field strengths because the heightened susceptibility effect magnifies phase variations [4] and does not suffer from the severe spatial distortions caused by off-

☆ The research was supported by UC Discovery grants LSIT01-10107 and ITL-BIO04-10148 in conjunction with GE Healthcare, NIH grants R01 CA059880 and P50 CA97257 and a Joelle Syverson American Brain Tumor Association Fellowship.

This work was presented in part at the 15th Annual Meeting of ISMRM, Berlin, Germany, 2007.

* Corresponding author. Tel.: +1 415 514 4420; fax: +1 415 514 2550.
E-mail address: janinel@radiology.ucsf.edu (J.M. Lupo).
[1] Current affiliation: GE Healthcare Applied Science Lab, Menlo Park, CA 94025, USA.

0730-725X/$ – see front matter. Published by Elsevier Inc.
doi:10.1016/j.mri.2008.08.003

resonance effects associated with echo planar imaging sequences. At 7 T, the enhanced sensitivity to microvasculature can provide a major advantage by allowing the detection of vessels as small as 100–200 μm. One of the disadvantages of this approach is that conventional SWI sequences involve long scan times due to the choice of repetition time (TR), which is influenced by the need to remove background image contrast from T_1 weighting, the signal-to-noise ratio (SNR) and requirement for high spatial resolution to visualize small vessels, despite the decrease in TE at higher field. This places a major emphasis on the need for a faster acquisition in order to improve coverage for a given spatial resolution while minimizing patient discomfort and motion-induced artifacts.

Partially parallel imaging (PPI) acquisitions and reconstruction algorithms [5–9] can be employed to accelerate long acquisition times as long as the concomitant decrease in SNR does not significantly affect the contrast between vessels and brain parenchyma. Direct techniques like Sensitivity Encoding (SENSE) [7] estimate the localized sensitivity of each coil element from a low-resolution coil calibration scan in order to unfold the aliased pixels in image space. This can be challenging in vivo at 7 T due to larger B_0 and B_1 spatial inhomogeneity. Indirect or autocalibrating (AC) techniques such as Generalized Autocalibrating Partially Parallel Acquisition (GRAPPA) obviate the need for explicit coil sensitivity estimation and allow for subsequent array combination [6,9–12]. GRAPPA is better suited to handle B_0/B_1 inhomogeneities than SENSE because the reconstruction is trained by the actual acquired data to generate the missing *k*-space lines, whereas the accuracy of SENSE relies on the accuracy of separate estimates of the receive coil sensitivity profiles, which is much more sensitive to B_0/B_1 inhomogeneities. Several variations in reconstruction filter kernel size and calibration procedure have been presented in the literature for GRAPPA-based reconstructions. These include performing the fitting piecewise for segments along the unaccelerated direction [11,12], floating node fitting (FNF), which allows additional data fits during the calibration [13], and a multicolumn multiline interpolation that also utilizes the nearest neighboring points in the frequency encode direction [13,14].

The possibility of using PPI techniques for accelerating the acquisition of SWI data has been proposed previously in the literature. Simulating elliptical and GRAPPA *k*-space undersampling and reconstruction regimes resulted in reduced vessel contrast at lower field strengths [13]. Our prior work in normal volunteers at 7 T found that a twofold acceleration with a GRAPPA-based technique could be achieved without compromising vessel contrast and provided images with improved contrast over SENSE-based reconstruction methods [14]. The goal of this study was to implement SWI at 7 T using a GRAPPA-based PPI technique and to demonstrate its utility in imaging brain tumors. The results were compared to the fully sampled acquisition in healthy controls and brain tumor patients and the SWI parameters adapted for improved visualization of vasculature, hemorrhage and radiation effects within regions of normal brain and tumor.

2. Methods

2.1. Data acquisition

High-resolution T_2*-weighted brain MR imaging was performed on 6 healthy volunteers and 11 patients with brain tumors using a 7 T whole-body MR scanner (GE Healthcare Technologies, Milwaukee, WI) with uniform excitation by a volume transmitter and reception by an eight-channel phased-array head coil (Nova Medical, Wilmington, MA). The SWI employed a 3D flow-compensated, SPGR sequence with nominal flip angle=20°, BW=62.5 kHz and FOV=24×24×2.8 cm^3. The optimal TE for maximum susceptibility contrast and image quality was determined empirically by scanning a range of TEs (8, 12, 16 and 20 ms) on a volunteer. The TR was subsequently shortened from 100 to 40 ms in 20-ms increments to find the minimum possible value that also maintained uniform contrast. A TE of 16 ms and TR of 80 ms resulted in the highest vessel contrast and image quality.

The fully sampled volunteer scans utilized a 512×256×28 (RL×AP×SI) image matrix, while the GRAPPA-based simulations and acquisitions employed either a 512×144×28 image matrix (for R=2) or a 512×102×28 image matrix (for R=3), with 16 AC lines. The imaging protocol included the acquisition of a low-resolution, proton-density-weighted, fast gradient echo sequence (TE/TR=2.1/150 ms, flip angle=20°, FOV=30×30 cm^2, image matrix=64×64 and slice thickness=3 mm) for coil sensitivity estimation. Of the 11 patient exams, 5 were acquired using a fully sampled acquisition. For the six patients who received a GRAPPA-based acquisition with R=2, the nearly twofold reduction in acquisition time was used to extend the coverage of the entire tumor. Informed consent was obtained from all patients and volunteers according to our institutional review board.

2.2. Reconstruction and postprocessing of complex multichannel data

The raw complex *k*-space data from all channels were transferred off-line to a Sun Blade 2000 Workstation (Sun Microsystems, Santa Clara, CA), and postprocessing was performed using in-house programs developed with Matlab 6.5 software (MathWorks Inc., Natick, MA) on a Linux cluster with four Sun Fire V20z AMD Opteron servers (2×2.4 GHz, 4 GB memory) running Sun's N1 Grid Engine. For the simulated volunteer scans, the fully sampled complex *k*-space data from each coil element were decimated in the phase-encoding direction to simulate reduction factors of 2 or 3, while retaining 16 central AC lines. The GRAPPA-based technique employed a 2D 4×3

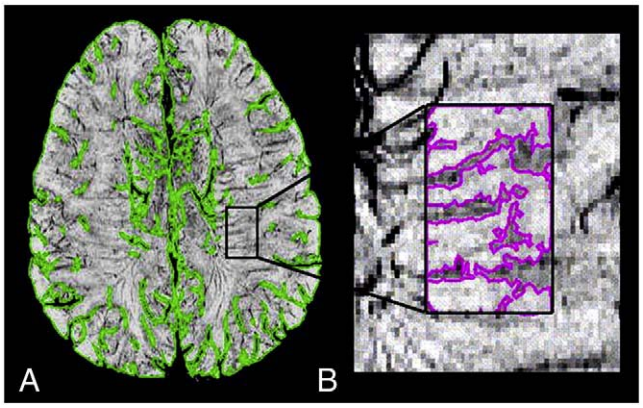

Fig. 1. Depiction of brain regions used to generate contrast ratios. In Panel A, there is a representative large vessel mask in green, while in Panel B, a region is enlarged to visualize a small vessel mask and neighboring white matter region, delineated in pink.

interpolation kernel using four neighboring points in the phase-encode direction, placed symmetrically around the missing line, and three neighboring data points in the frequency encode axis as FNF points [15]. SWI post-processing was then performed on the zero-filled complex *k*-space data on a coil-by-coil basis once the missing lines were synthesized.

SWI utilized the phase information from the complex signal to reduce the signal intensity from venous vessels in the magnitude images. Phase masks were constructed from the full complex *k*-space data of each individual coil element (after the GRAPPA-based reconstruction of the missing *k*-space lines) through complex division by a low-pass filtered image and scaling the resulting negative phase values between zero and one [1]. The phase masks were then multiplied with the magnitude image from each channel *m* times, and the resulting susceptibility-weighted images from each channel were combined by either the traditional square root of sum of squares (SOS) method, scaling the data by the variance of its noise for each channel, or summing images weighted by normalized coil sensitivity profiles [16]. For volunteer data, a 64×64 Hanning filter with m=4 weighting was employed. A range of *k*-space window filter sizes was explored for the patient scans, and a 128×128 point low-pass filter was found to remove the higher-frequency wraps that occurred due to prior surgical resection around the tumor region. In this case, the number of multiplications by the phase mask (m) was increased from four to six to elevate the reduced susceptibility weighting from the larger filter size while minimizing the amount of noise amplification in the final image. A low-pass filter with edge completion [17] was applied to the combined images to minimize any residual intensity variation across the image. Minimum intensity projections (mIPs) through 15-mm-thick slabs of similar anatomical locations were generated to obtain the SWI images that were used in the subsequent analysis.

2.3. Data analysis

Contrast ratios of the undersampled data sets were compared to the fully sampled case. The choice of contrast ratios for the analysis of patient data was driven by the need to have comparable metrics to the values in normal volunteers within the available scan time. Vessel contrast was estimated from the mIPs of the susceptibility-weighted images using masks of large and small vessels and surrounding brain tissue generated by thresholding the SWI mIP images at varying degrees, removing disconnected pixels and filling-in isolated interior pixels (Fig. 1). A different set of thresholds was utilized for each acquired SWI image, and the resulting masks were applied to subsequent simulated undersampled images. Contrast ratios were calculated from the mean signal intensity within each brain mask divided by that of the corresponding vessel mask. The brain parenchyma region was used as the background calculation of large vessel contrast and adjacent white matter as the background for detecting small vessels. Statistical significance among simulated data sets within the same volunteer was evaluated using a Wilcoxon signed-rank test, and comparisons between patient groups used a Wilcoxon rank sum test.

SNR and CNR values were also calculated in the two acquired normal volunteers for whom the necessary repeat scans were available. The SNR was calculated from the preprocessed magnitude images of two repeated scans for each acquisition on one volunteer data set using the two-repetition method described by Dietrich et al. [18], where the average SNR in a given ROI is determined as the ratio of average signal in the mean image and the standard deviation of the signal in the difference image. The CNR calculation divided the change in signal intensity in the small vessels from the surrounding white matter tissue by the standard deviation of the signal in the difference image of the final min-mipped SWI image.

Table 1
Large and small vessel contrast ratios and SNR for each acquisition

	Fully sampled	GRAPPA (R=2)	GRAPPA (R=3)
Volunteer data			
Simulated mean lv CR	4.36±0.79	4.35±0.82	4.27±0.79
Acquired lv CR (1)	3.58	4.13	4.27
Acquired lv CR (2)	4.01	4.43	4.34
Simulated mean sv CR	1.34±0.09	1.30±0.09	1.29±0.09
Acquired sv CR (1)	1.18	1.27	1.33
Acquired sv CR (2)	1.37	1.34	1.32
Scan time	10:59	6:12	4:25
SNR	29.5	18.4	15.0
Patient data			
Mean lv CR (f64, m4)	3.96±0.40	4.22±1.24	–
Mean lv CR (f128, m6)	4.02±0.43	4.10±1.28	–
Mean sv CR (f64, m4)	1.40±0.05	1.38±0.14	–
Mean sv CR (f128, m6)	1.48±0.06	1.45±0.19	–

CR, contrast ratio; lv, large vessel; sv, small vessel; f, filter size; m, number of multiplications.

3. Results

3.1. Simulated GRAPPA-based volunteer data

The mean contrast ratios for fully sampled and simulated GRAPPA-based data from normal volunteers are displayed in Table 1. There was no statistically significant difference in large vessel contrast ($P>.2$, Wilcoxon signed-rank test) between the GRAPPA $R=2$ and fully sampled acquisitions, but a 2.8% reduction in small vessel contrast was observed ($P<.02$). Simulating an $R=3$ reduction resulted in a 1.9% decrease in large vessel contrast compared to that of the $R=2$ acquisition ($P<.02$), but the small vessel contrast remained relatively constant ($P>.2$).

Vessel contrast ratios were also sensitive to the method of coil combination as shown in Fig. 2. When using a weighted sum of coil sensitivity profiles for coil combination [16], 11% and 15% decreases in large and small vessel contrast were observed for the fully sampled acquisition compared to the SOS combination ($P<.05$). For GRAPPA-based data sets, a 2% increase in large vessel contrast was detected when using the coil sensitivity profiles to combine the data ($P<.05$). A 2% increase in large vessel contrast persisted when weighting by the noise variance of each coil ($P<.05$), with no effect on small vessel contrast. Visual assessment of the combined images showed greatest uniformity when weighting by the noise variance of each channel.

3.2. Acquired GRAPPA-based volunteer data

Data were acquired for two volunteers with scan times of 10 min 59 s, 6 min 12 s and 4 min 25 s for the fully sampled

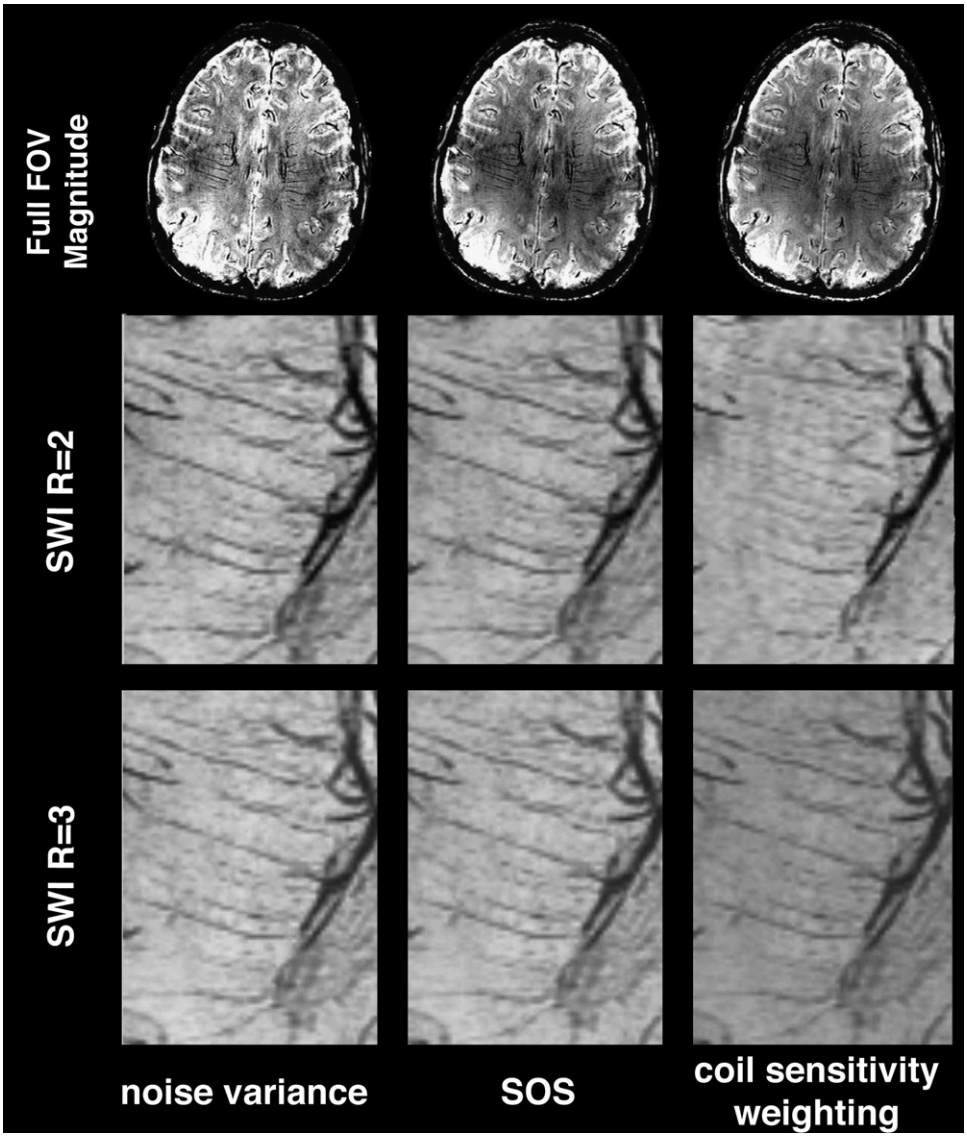

Fig. 2. Effects of coil combination method on vessel contrast for the fully sampled and reduced sampled images. The top row shows uncorrected combined magnitude images with greatest uniformity when weighting solely by the noise variance of each coil. In the lower two rows, the enlarged images demonstrate the reduced small vessel contrast observed when using a weighted sum of coil sensitivity profiles for coil combination.

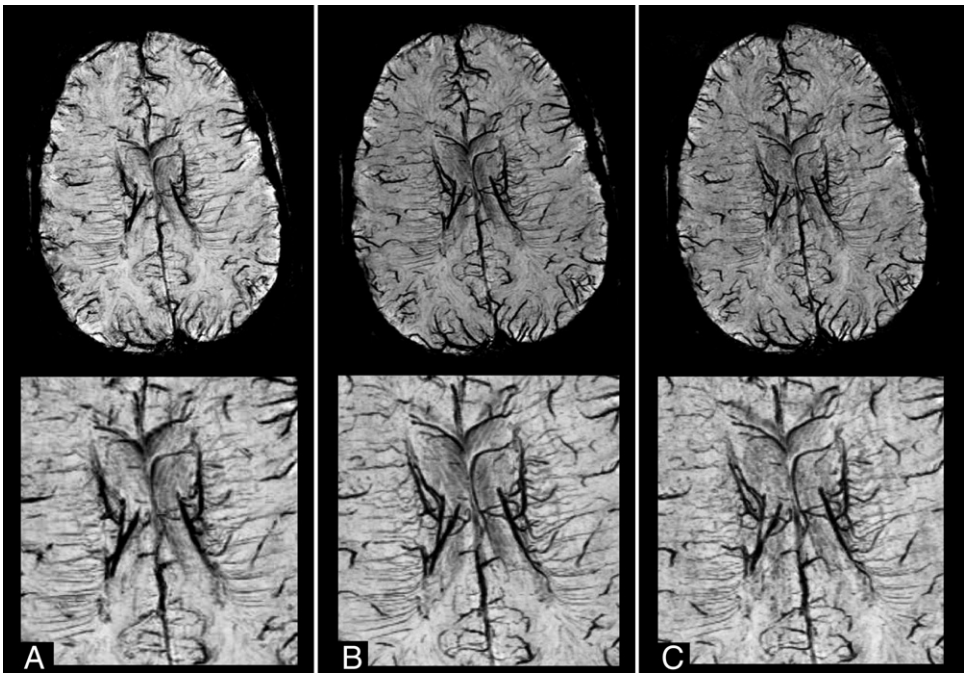

Fig. 3. Acquired normal volunteer SWI with a mIP of 15 mm for the (A) fully sampled, (B) twofold reduction (R=2) and (C) threefold reduction (R=3) acquisitions. The bottom row displays magnified SWI images for the visualization of small vessels.

k-space, a reduction factor of R=2 and a reduction factor of R=3, respectively. The R=3 acquisition results in a 2.5-fold decrease in scan time, rather than a threefold acceleration, because of the additional AC lines required for GRAPPA. Fig. 3 depicts SWI images comparing two- and threefold accelerations to the fully sampled data set for a representative volunteer. Visual inspection demonstrates similar vessel contrast between the fully sampled and R=2 acquisitions. For the R=3 acquisition, there was no visible disparity in large vessel contrast compared to the fully sampled and R=2 scans, but the visibility of small vessels was slightly hindered. Small vessel contrast ratios for the R=3 acquired data sets were similar to those from the R=2 scans. SNR measurements revealed a 37.6% decrease in SNR for the R=2 acquisition, with a 43.1% reduction in total scan time. The R=3 scan showed a 49.3% decline in SNR, with a reduction of 60% in scan time. CNR values for small vessels varied at least 43% depending on the spatial location, while contrast ratios only exhibited an 8% deviation in values obtained from different regions throughout the brain and more accurately characterized the visual appearance of these vessels (Fig. 4).

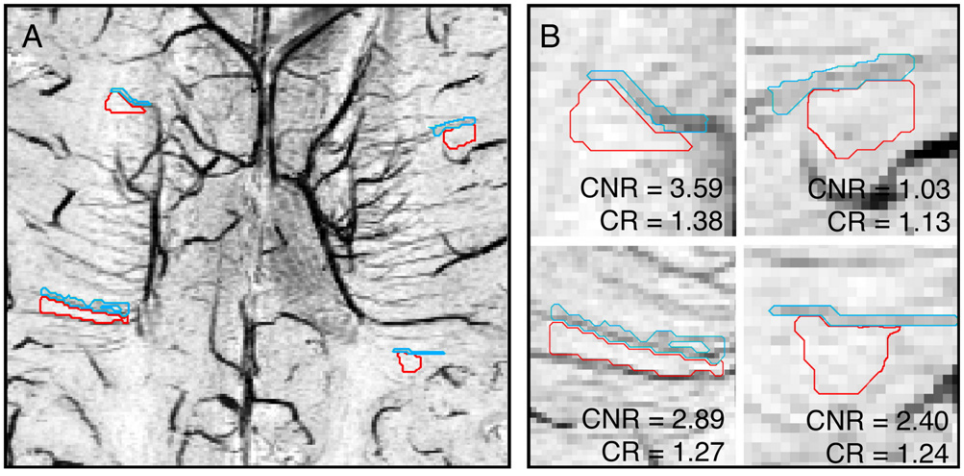

Fig. 4. Variation of CNR and stability of contrast ratio (CR) across the head in a representative normal volunteer acquired with the R=2 acquisition. In Panel A, small vessel (blue) and adjacent white matter (red) regions in four different brain locations are shown. In Panel B, the regions from Panel A are magnified to show the apparent similarity in contrast despite the variation in CNR values.

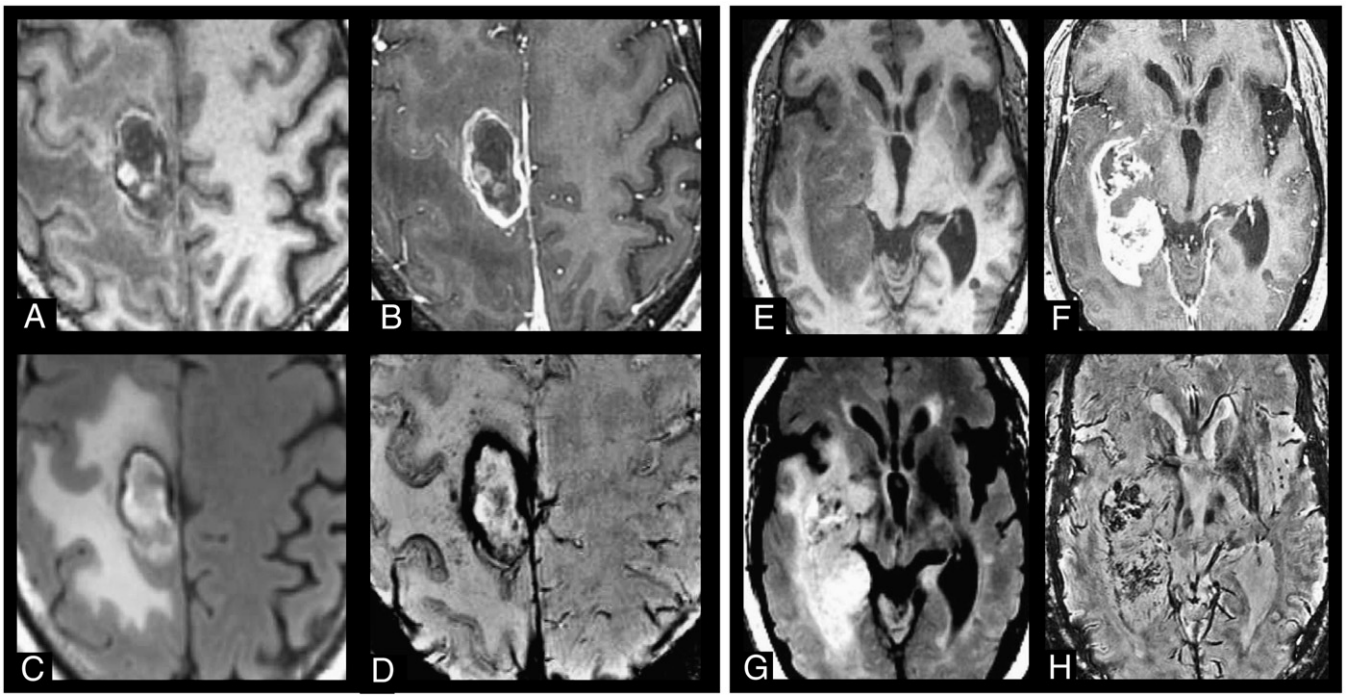

Fig. 5. Illustration of fully sampled and GRAPPA-based SWI of brain tumors compared to corresponding 3-T anatomical images. In the left panel, a recurrent glioma patient post-therapy with (A) pre-Gd T_1-weighted SPGR, (B) post-Gd T_1-weighted SPGR, (C) T_2-weighted FLAIR imaging at 3 T and (D) fully sampled SWI at 7 T. In the right panel, a newly diagnosed glioma patient pre-therapy with (E) pre-Gd T_1-weighted SPGR, (F) post-Gd T_1-weighted SPGR, (G) T_2-weighted FLAIR imaging at 3 T and (H) GRAPPA-based SWI (R=2) at 7 T.

3.3. GRAPPA-based SWI of brain tumor patients

Similar contrast ratios were observed for the patients with brain tumors when projected at the same thickness as the data from the volunteers (P>.1, Wilcoxon rank sum test). Large and small vessel contrasts were similar between patient cohorts with the fully sampled and R=2 acceleration (P>.5). Fig. 4 shows representative SWI images of brain tumors for the fully sampled and R=2 acquisitions and corresponding anatomical imaging obtained from a subsequent 3 T scan. The right-hand panel portrays an untreated patient with high-grade glioma, where the SWI is able to highlight regions of chronic hemorrhage or calcification in portions of the contrast-enhancing lesion. The left-hand side of Fig. 5 illustrates additional contrast within a Grade III glioma after having received radiation and chemotherapy. A hemosiderin ring following the majority of the contrast-enhancing rim lesion on the post-gad T_1-weighted 3 T images and microhemorrhages within the surrounding edema both show marked hypointensity on the SWI image, whereas regions of acute hemorrhage with T_1 hyperintensity on the pre-gad 3 T images also appear hyperintense on the SWI. Fig. 6 further demonstrates the utility of GRAPPA-based SWI at 7 T by illustrating microhemorrhages in normal brain tissue due to radiation, the recruitment of large blood vessels in active tumor regions and the accumulation of blood products. The 7 T SWI provides additional contrast both within the enhancing tumor lesion and surrounding edema, and performing a mIP is not always necessary to visualize vessels, blood products or radiation effects in the tumor region.

Although similar vessel contrast was observed in brain tumor patients as healthy volunteers, the presence of higher-frequency phase wraps arising from susceptibility-induced phase changes from surgical resection or heterogeneous tumor tissue would have contaminated image quality in 8 out of 11 patients if the same postprocessing parameters were used. To accommodate this, the filter kernel size and number of mask multiplications were altered to minimize the number of residual phase wraps in these regions while maintaining heightened vessel contrast. Small vessel contrast was heightened by 5% with increased filter size and m value in all patients (Table 1, P<.05), with no significant difference in large vessel contrast (P>.5, Wilcoxon signed-rank test). The additional noise from the increased multiplications was not visually apparent in the final SWI images although the standard deviation of image intensity within the normal brain region increased by 7% and 10% (P<.05) for the fully sampled and R=2 acquisitions, respectively.

4. Discussion

This study has shown the feasibility and highlighted the potential benefits of using a GRAPPA-based acquisition and reconstruction to accelerate susceptibility-weighed imaging

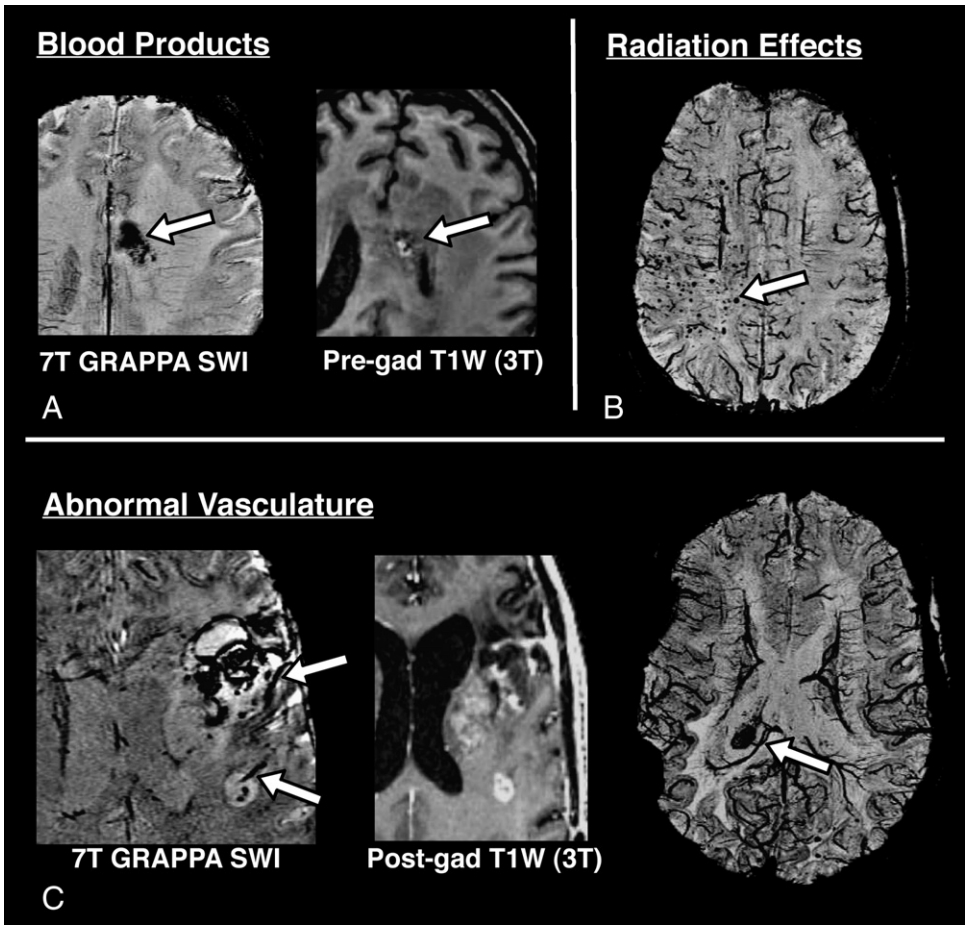

Fig. 6. Depiction of (A) blood products, (B) radiation effects and (C) abnormal vasculature in treated brain tumors using SWI at 7 T. The two dark areas at the brain's surface in the image on the right in Panel C are due to artifacts from surgical excision.

at 7 T in normal volunteers and patients with brain tumors. The implementation of parallel imaging with GRAPPA-based reconstruction can allow at least a twofold reduction in scan time without significantly compromising the contrast between veins and surrounding brain tissue. This may be used to either increase coverage or reduce scan time without impinging on spatial resolution.

The ability to visualize the vessels in SWI is influenced by two factors. The first is the intrinsic contrast in the magnitude images, which shows vessels as being darker and is influenced by the contrast in the vessels. The second is the weighting provided by the phase of the image at each pixel and which increases local contrast relative to surrounding tissue. The latter is highly dependent on the SNR of the images and accentuates the contrast in the weighted image when the mean signal in the vessel and the mean of the background regions of interest are close in value. Although CNR values are commonly reported to assess image quality, it was not the best choice of metrics for this study due to the variation of noise throughout the head, which was even further exacerbated by both the reconstruction and numerous postprocessing calculations (i.e., coil combination, high- and low-pass filtering, multiplications and projections) applied to create the images. Further studies are necessary to explore the effects of each of these processing steps on the distribution of noise before measures such as CNR can be considered the standardized metric to compare GRAPPA-based SWI images. In this study, contrast ratios were a much more stable, reproducible measure that more accurately reflected the contrast visually perceived in these images, with only an 8% deviation in values obtained from varying spatial locations (Fig. 4).

The size of vessels experiencing diminished contrast ratios was shown to increase with higher reduction factors. For simulated data sets, larger vessels did not exhibit lower contrast compared to surrounding tissue until a threefold reduction factor (or 2.5-fold acceleration in scan time) was implemented, but smaller vessels began to lose contrast after a twofold reduction in *k*-space sampling. This effect was most likely due to the associated decreased SNR. There were no significant differences in contrast for the two normal volunteers and patients scanned with accelerated acquisitions relative to the patients with data acquired using full *k*-space sampling for both vessel sizes. One possible explanation for there being differences in significance between the simulated and empirical data is that the methods for defining the phase

mask varied. For the simulated data sets, the mask was generated from the fully sampled acquisition and then subsequently applied to the reduced data sets. For scans with reduced *k*-space sampling, it was necessary to create a new set of masks for each acquisition in order to compensate for any motion or misalignment that might have occurred between full and reduced data acquisitions. This meant that the difference in contrast among the reduced acquisitions in the normal volunteer data sets could not be directly compared in the same way as for the simulated data sets. The contrast ratios for acquired GRAPPA-based scans were within the range of values obtained from the simulated data in all cases.

Comparisons of vessel contrast ratios were further influenced by the method of coil combination. A weighted sum combination should yield similar or elevated vessel contrast compared to SOS due to the increase in SNR inherent with this combination. However, this was only true for large vessel contrast at higher reduction factors. Contrary to what was expected, the SOS combination had improved small vessel contrast compared to the weighted sum combination. This suggests that a higher-resolution coil sensitivity profile is required to improve the contrast of smaller vessels in the weighted sum combination. For both the fully sampled and GRAPPA-based data sets, weighting by the noise variance of each coil seemed to improve large vessel contrast without adversely affecting the detection of smaller vessels. This may be due to the difference in noise amplification among receive coils dominating the balance between the decrease in signal intensity away from the coil elements and the heightened signal due to the dielectric effect in the center of the head that exists for a circularly symmetric array of coils at high field strengths.

The acquisition parameters utilized in this study were selected to optimize vessel contrast and overall image quality in normal volunteers and were then held constant for applications to patients with brain tumors. This meant that the patient data may not always have been acquired with the best possible acquisition parameters and that some of the postprocessing parameters needed to be altered. The greatest problem when transitioning from normal volunteer to brain tumor patients was the higher-frequency phase wraps that arose from susceptibility-induced phase changes caused by surgical resection or heterogeneity within the tumor itself. The simplest postprocessing solution to remove this artifact was to increase the size of the *k*-space windowing filter. Since the resulting phase mask is more high-pass filtered, a larger number of multiplications is necessary to achieve the same contrast. The trade-off is a decrease in SNR caused by amplification of noise from the increased multiplications. This was evident in the elevated standard deviations observed within each mask. Alternative methods to stronger *k*-space filtering for the removal of phase wraps [19], although more challenging at 7 T due to the higher-frequency phase wraps and the reduced SNR introduced with parallel imaging, may also be explored. Although shorter TEs could be utilized to minimize residual phase wrapping artifacts, a shorter TE would result in decreased contrast and susceptibility weighting and not necessarily decrease scan times since a longer TR is still necessary to remove any background image contrast due to T_1 weighting that would obscure vessel contrast. Future optimization of these parameters in a heterogeneous cohort of brain tumor patients would help determine which combination of TE and filter selection minimizes the number of phase wraps and maximizes both SNR and susceptibility contrast.

In conclusion, we have demonstrated the feasibility of implementing a GRAPPA-based SWI method at 7 T, with up to a 2.5-fold reduction in scan time in normal volunteers without significantly diminishing vessel contrast. The heightened contrast achieved at 7 T is a 1.4- and 1.2-fold improvement over 3 T for large and small vessels [20]. Large brain tumor lesions were covered in less than 7 min, facilitating the incorporation of this technique into routine patient studies. The preliminary results obtained with SWI at 7 T suggest that unique forms of contrast may be useful for assessing response to both radiation and antiangiogenic therapies for patients with brain tumors. Future increases in slice thickness to 2 mm, as recently described by Xu and Haacke [21] as the best voxel aspect ratio for the visualization of veins, will improve both SNR and coverage, allowing for decreased flip angles and TRs to further shorten scan time.

References

[1] Haacke EM, Xu Y, Cheng YC, Reichenbach JR. Susceptibility weighted imaging (SWI). Magn Reson Med 2004;52(3):612–8.
[2] Sehgal V, Delproposto Z, Haacke EM, Tong KA, Wycliffe N, Kido DK, et al. Clinical applications of neuroimaging with susceptibility-weighted imaging. J Magn Reson Imaging 2005;22(4):439–50.
[3] Sehgal V, Delproposto Z, Haddar D, Haacke EM, Sloan AE, Zamorano LJ, et al. Susceptibility-weighted imaging to visualize blood products and improve tumor contrast in the study of brain masses. J Magn Reson Imaging 2006;24(1):41–51.
[4] Ladd ME. High-field-strength magnetic resonance: potential and limits. Top Magn Reson Imaging 2007;18(2):139–52.
[5] Blaimer M, Breuer F, Mueller M, Heidemann RM, Griswold MA, Jakob PM. SMASH, SENSE, PILS, GRAPPA: how to choose the optimal method. Top Magn Reson Imaging 2004;15(4):223–36.
[6] Griswold MA, Jakob PM, Heidemann RM, Nittka M, Jellus V, Wang J, et al. Generalized autocalibrating partially parallel acquisitions (GRAPPA). Magn Reson Med 2002;47(6):1202–10.
[7] Pruessmann KP, Weiger M, Scheidegger MB, Boesiger P. SENSE: sensitivity encoding for fast MRI. Magn Reson Med 1999;42 (5):952–62.
[8] Sodickson DK, Manning WJ. Simultaneous acquisition of spatial harmonics (SMASH): fast imaging with radiofrequency coil arrays. Magn Reson Med 1997;38(4):591–603.
[9] Heidemann RM, Griswold MA, Haase A, Jakob PM. VD-AUTO-SMASH imaging. Magn Reson Med 2001;45(6):1066–74.
[10] Jakob PM, Griswold MA, Edelman RR, Sodickson DK. AUTO-SMASH: a self-calibrating technique for SMASH imaging. SiMultaneous Acquisition of Spatial Harmonics. Magma 1998;7(1):42–54.
[11] Park J, Zhang Q, Jellus V, Simonetti O, Li D. Artifact and noise suppression in GRAPPA imaging using improved *k*-space coil

calibration and variable density sampling. Magn Reson Med 2005;53 (1):186–93.
[12] Wang Z, Wang J, Detre JA. Improved data reconstruction method for GRAPPA. Magn Reson Med 2005;54(3):738–42.
[13] Sedlacik J, Herrmann K, Rauscher A, Reichenbach JR. SWI using different *k*-space undersampling mechanisms. Proceedings from the 13th Annual International Society for Magnetic Resonance in Medicine Meeting. May 7–13, Miami, FL,; 2005.
[14] Lupo JM, Barnerjee S, Kelley DAC, Xu D, Vigneron DB, Majumdar S, et al. Partially-parallel, susceptibility-weighted MR imaging of brain vasculature at 7 Tesla using sensitivity encoding and an autocalibrating parallel technique. Proceedings from the 28th Annual International Conference of the IEEE-EMBS. August 30–September 3, New York, NY; 2006.
[15] Banerjee S, Choudhury S, Han ET, Brau AC, Morze CV, Vigneron DB, et al. Autocalibrating parallel imaging of in vivo trabecular bone microarchitecture at 3 Tesla. Magn Reson Med 2006;56(5):1075–84.
[16] Bydder M, Larkman DJ, Hajnal JV. Combination of signals from array coils using image-based estimation of coil sensitivity profiles. Magn Reson Med 2002;47(3):539–48.
[17] Wald LL, Carvajal L, Moyher SE, Nelson SJ, Grant PE, Barkovich AJ, et al. Phased array detectors and an automated intensity-correction algorithm for high-resolution MR imaging of the human brain. Magn Reson Med 1995;34(3):433–9.
[18] Dietrich O, Reeder S, Reiser MF, Schoenberg SO. Influence of parallel imaging and other reconstruction techniques on the measurement of signal-to-noise ratios. Proceedings from the 13th Annual International Society for Magnetic Resonance in Medicine Meeting. May 7–13; 2005. p. 158. [Miami, FL].
[19] Rauscher A, Barth M, Reichenbach JR, Stollberger R, Moser E. Automated unwrapping of MR phase images applied to BOLD MR-venography at 3 Tesla. J Magn Reson Imaging 2003;18(2):175–80.
[20] Lupo JM, Kelley DAC, Xu D, Vigneron DB, Nelson SJ. Susceptibility-weighted imaging at 3T and 7T using multi-channel phased array coils and SENSE. Proceedings of the 14th Annual Meeting of the International Society for Magnetic Resonance in Medicine. May 8–12, Seattle, WA; 2006.
[21] Xu Y, Haacke EM. The role of voxel aspect ratio in determining apparent vascular phase behavior in susceptibility weighted imaging. Magn Reson Imaging 2006;24(2):155–60.